Optical Single-Sideband Modulation Based on a Dual-Drive MZM and a 120° Hybrid Coupler

Min Xue, Shilong Pan, *Senior Member, IEEE, Member, OSA*, and Yongjiu Zhao

***Abstract*—A novel scheme for implementing high-performance optical single-sideband (OSSB) modulation based on a dual-drive Mach–Zehnder modulator (MZM) and a 120° hybrid coupler is proposed and demonstrated. A RF signal is divided by the 120° hybrid coupler into two parts with equal powers and a phase difference of 120°, and then, led to the two RF ports of the dual-drive MZM. With a proper dc bias, an OSSB signal with the −1st and +2nd-order sidebands (or the +1st and −2nd-order sidebands) suppressed is generated. A numerical simulation and a proof-of-concept experiment are carried out. As compared with the conventional OSSB modulation based on a 90° hybrid coupler, the suppression of the +2nd (or −2nd)-order sideband improves evidently the performance when the OSSB modulation is applied in a radio-over-fiber system or an optical vector network analyzer.**

***Index Terms*—Microwave photonics, optical single-sideband (OSSB) modulation, optical vector network analysis, radio-over-fiber (RoF).**

I. Introduction

OPTICAL single-sideband (OSSB) modulation has become an attractive technology for long-distance radio-over-fiber (RoF) system [1], [2], high-accuracy optical sensing [3], high-resolution optical vector network analysis [4]–[9], optical wavelength conversion [10], and optical coherence tomography [11]. For example, the OSSB signal is free from the frequency-dependent power fading induced by fiber dispersion, which is a serious problem in the conventional double-sideband (DSB) modulated RoF system. Previously, several schemes for implementing the OSSB modulation were reported [12]–[19], which can be classified into two main categories, namely, optical filtering method and 90° phase shift method. In the optical filtering method, the OSSB signal is generated by removing one of the first-order sidebands in an intensity-modulated (IM) or phase-modulated (PM) signal. Uniform fiber Bragg grating (FBG) [12], phase shift fiber Bragg grating (PS-FBG) [13], steep-edge tunable optical filter [6], crystalline whispering gallery mode resonator [14], or active photonic filter based on stimulated Brillouin scattering (SBS) [15] was employed to implement the OSSB modulation. However, the method is highly dependent on the wavelength of the optical carrier. In addition, if a wide-band optical filter is used, it is difficult to eliminate one first-order sideband without affecting the optical carrier and the other sidebands, and if a narrow bandwidth optical filter is applied, the OSSB modulation can only realized in a small frequency range.

Manuscript received March 26, 2013; revised December 3, 2013 and March 29, 2014; accepted July 21, 2014. Date of publication July 30, 2014; date of current version August 27, 2014. This work was supported in part by the National Natural Science Foundation of China under Grant 61107063, the National Basic Research Program of China (2012CB315705), the Aviation Science Foundation of China under Grant 2012ZD52052, the Jiangshu Provincial Funds for Distinguished Young Scientists under Grant BK2012031, the Jiangsu Provincial Program for High-level Talents in Six Areas under Grant DZXX-034, the Fundamental Research Funds for the Central Universities, Funding of Jiangsu Innovation Program for Graduate Education under Grant CXZZ12_0154, Funding for Outstanding Doctoral Dissertation in NUAA under Grant BCXJ13-08, and the Foundation of Graduate Innovation Center in Nanjing University of Aeronautics and Astronautics under Grant KFJJ20130214.

The authors are with the Key Laboratory of Radar Imaging and Microwave Photonics, Ministry of Education, Nanjing University of Aeronautics and Astronautics, Nanjing 210016, China (e-mail: xueminnat@gmail.com; pans@ieee.org; yjzhao@nuaa.edu.cn).

Color versions of one or more of the figures in this paper are available online at http://ieeexplore.ieee.org.

Digital Object Identifier 10.1109/JLT.2014.2344853

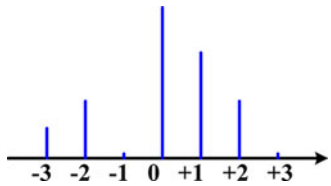

Fig. 1. Typical optical spectrum of the OSSB-modulated signal based on a 90° hybrid coupler.

In contrast, the OSSB modulation realized by the 90° phase shift method is almost independent of the wavelength of the optical carrier. In that method, two RF signals with a phase difference of 90° are introduced to a dual-drive Mach–Zehnder modulator (MZM) [16] or a dual-parallel MZM (DPMZM) [17]. The optical components in the upper and lower arms of the MZM have a phase difference of $n \times \pi/2 - \phi_0$, where n represents the order of the sideband and ϕ_0 is an additional phase difference introduced by the dc bias. With $\phi_0 = -\pi/2$ or $\pi/2$ by properly setting the dc bias, one of the first-order sidebands would be destructively interfered when the two optical signals in the upper and lower arms are combined at the output port of the modulator. An OSSB-modulated signal is thus generated. A typical optical spectrum of the OSSB-modulated signal based on a 90° hybrid coupler is shown in Fig. 1. By letting $\phi_0 = -\pi/2$, the −1st and +3rd-order sidebands are effectively suppressed. But the unwanted +2nd and higher order sidebands still exist especially when the system relies on relatively large phase modulation index to improve the optical-to-electrical conversion efficiency. In a long-reach RoF system, the existence of the +2nd-order sideband would make the signal quasi-DSB, which will undergo some frequency-dependent power penalty due to the fiber dispersion. In addition, in an OSSB-based optical vector network analyzer, the component beat by the +1st and +2nd-order sidebands contributes a considerable proportion of the fundamental beat component, which results in appreciable measurement error as indicated in one of our previous works [20]. This error would

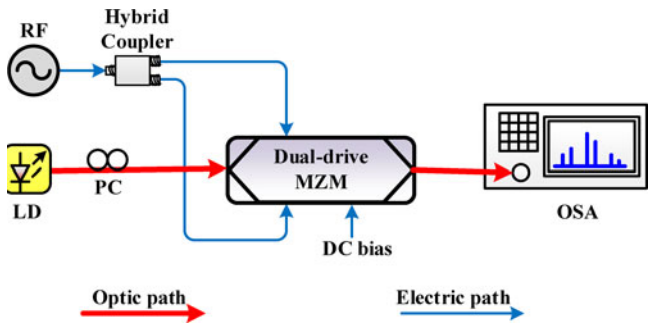

Fig. 2. The schematic diagram of OSSB modulation based on a hybrid coupler and a dual-drive MZM. LD: laser diode; PC: polarization controller; RF: radio frequency; MZM: Mach–Zehnder modula.

also lead to the inaccurate measurement of the polarization dependent loss (PDL), polarization mode dispersion (PMD), and group delay [8]. To overcome these problems, it is highly desirable that the +2nd-order sideband is eliminated.

In this paper, a novel OSSB modulation based on a 120° hybrid coupler and a dual-drive Mach–Zehnder modulator is proposed and demonstrated. In the scheme, the optical signals in the upper and lower arms of the dual-drive MZM have a phase difference of $n \times 2\pi/3 - \phi_0$. When $\phi_0 = \pi/3$, which is implemented by properly setting the dc bias, the −1st-order sideband, i.e., $n = -1$, is suppressed because the −1st-order sidebands in the two arms of the modulator have a −180° phase difference and are destructively interfered when combined at the output port of the MZM. Simultaneously, the +2nd-order sidebands, i.e., $n = +2$, are also destructively interfered owing to the +180° phase difference. As a result, an OSSB signal with both of the −1st and +2nd-order sidebands suppressed is generated. Similarly, when $\phi_0 = -\pi/3$, an OSSB signal with both of the +1st and −2nd-order sidebands suppressed is generated. The comparative numerical study of the OSSB modulation based on the 90° and 120° hybrid couplers is performed. The +2nd-order sideband of the proposed OSSB modulation based on a 120° hybrid coupler is suppressed by 26.38 dB compared with that of the conventional OSSB modulation based on a 90° hybrid coupler at a phase modulation index of $\pi/3$. When applying in the high-resolution optical vector network analysis, the simulation results show that the transmission function measured by the proposed OSSB modulation is much more accurate than that measured by the conventional approach. The comparison of the performance of the two OSSB modulations in a RoF system with 20-km single mode fiber (SMF) is also experimentally evaluated. When the RF signal is modulated by a 50 Mbaud 16 QAM signal, the error vector magnitudes (EVMs) of the 90° and 120° hybrid couplers based OSSB signals are degraded by 0.5472% and 0.3825%, respectively, showing that the proposed OSSB modulation has better transmission performance.

II. Analytical Analysis

Fig. 2 shows a typical configuration of the OSSB modulation based on a hybrid coupler and a dual-drive MZM. An optical carrier from a laser diode (LD) is fed to the optical port of the dual-drive MZM. A RF signal is divided by a hybrid coupler into two parts with equal powers and a phase difference of φ, which are then led to the two RF ports of the dual-drive MZM. With a proper dc bias, an additional phase difference of ϕ_0 is introduced between the optical signals in the upper and lower arms.

Assuming that the optical carrier from the LD is $E_c \exp(i\omega_c t)$, the optical field of the modulated signal can be written as

$$\begin{aligned} E(t) = {} & E_{\mathrm{c}} \exp(i\omega_{\mathrm{c}} t) \{\exp[i\beta_1 \cos(\omega_{\mathrm{e}} t + \varphi)] \\ & + \exp[i\beta_2 \cos(\omega_e t) + i\phi_0]\} \end{aligned} \tag{1}$$

where β_1 and β_2 are the phase modulation indices in the two arms, ω_e is the angular frequency of the modulating signal. Based on the Jacobi–Anger expansion, (1) can be rewritten as

$$\begin{aligned} E(t) = {} & \sum_{m=-\infty}^{\infty} E_{\mathrm{c}} i^m \{J_m(\beta_1) \exp[i(\omega_{\mathrm{c}} + m\omega_{\mathrm{e}})t + im\varphi] \\ & + J_m(\beta_2) \exp[i(\omega_{\mathrm{c}} + m\omega_{\mathrm{e}})t + i\phi_0]\} \\ = {} & \sum_{m=-\infty}^{\infty} E_{\mathrm{c}} i^m \exp[i(\omega_c + m\omega_{\mathrm{e}})t] \\ & \{J_m(\beta_1) \exp(im\varphi) + J_m(\beta_2) \exp(i\phi_0)\} \end{aligned} \tag{2}$$

where $J_m(\beta)$ is the mth order of the Bessel function of the first kind.

Since the −2nd, −1st, 0th, +1st and +2nd-order sidebands are of the most importance to the OSSB modulation, we list the optical fields of these sidebands as follows:

$$\begin{aligned} E_{-2} = {} & E_{\mathrm{c}} \exp(i\pi)[J_2(\beta_1) \exp(-i2\varphi) + J_2(\beta_2) \exp(i\phi_0)] \\ & \exp[i(\omega_c t - 2\omega_e t)] \\ E_{-1} = {} & E_{\mathrm{c}} \exp\left(i\frac{\pi}{2}\right)[J_1(\beta_1) \exp(-i\varphi) + J_1(\beta_2) \exp(i\phi_0)] \\ & \exp[i(\omega_c t - \omega_e t)] \\ E_0 = {} & E_{\mathrm{c}}[J_0(\beta_1) + J_0(\beta_2) \exp(i\phi_0)] \exp(i\omega_c t) \\ E_{+1} = {} & E_{\mathrm{c}} \exp\left(i\frac{\pi}{2}\right)[J_1(\beta_1) \exp(i\varphi) + J_1(\beta_2) \exp(i\phi_0)] \\ & \exp[i(\omega_c t + \omega_e t)] \\ E_{+2} = {} & E_{\mathrm{c}} \exp(i\pi)[J_2(\beta_1) \exp(i2\varphi) + J_2(\beta_2) \exp(i\phi_0)] \\ & \exp[i(\omega_c t + 2\omega_e t)]. \end{aligned} \tag{3}$$

The corresponding optical powers are

$$\begin{aligned} P_{-2} &= E_{\mathrm{c}}^2 \left[J_2^2(\beta_1) + J_2^2(\beta_2) + 2J_2(\beta_1)J_2(\beta_2)\cos(2\varphi + \phi_0)\right] \\ P_{-1} &= E_{\mathrm{c}}^2 \left[J_1^2(\beta_1) + J_1^2(\beta_2) + 2J_1(\beta_1)J_1(\beta_2)\cos(\varphi + \phi_0)\right] \\ P_0 &= E_{\mathrm{c}}^2 \left[J_0^2(\beta_1) + J_0^2(\beta_2) + 2J_0(\beta_1)J_0(\beta_2)\cos(\phi_0)\right] \\ P_{+1} &= E_{\mathrm{c}}^2 \left[J_1^2(\beta_1) + J_1^2(\beta_2) + 2J_1(\beta_1)J_1(\beta_2)\cos(\varphi - \phi_0)\right] \\ P_{+2} &= E_{\mathrm{c}}^2 \left[J_2^2(\beta_1) + J_2^2(\beta_2) + 2J_2(\beta_1)J_2(\beta_2)\cos(2\varphi - \phi_0)\right] \end{aligned} \tag{4}$$

To achieve an OSSB modulation with the −1st and +2nd-order sidebands suppressed, the following conditions should be

satisfied

$$\begin{cases} \beta_1 = \beta_2 \\ \cos(\varphi + \phi_0) = -1 \\ \cos(2\varphi - \phi_0) = -1. \end{cases} \tag{5}$$

From (5), we have $\beta_1 = \beta_2, \varphi = 2\pi/3$, and $\phi_0 = \pi/3$. Thus, the OSSB modulation can be realized by a 120° (i.e., $2\pi/3$) hybrid coupler and a dual-drive MZM by a proper dc bias, which introduces an additional phase difference of $\pi/3$ between the two arms of the dual-drive MZM. It should be noted that a wideband 120° hybrid coupler can be achieved by coupling between the top and bottom elliptical microstrip patches via an elliptical slot located in the mid-layer [22] or the microstrip-lines connected to a low-impedance rectangular microstrip patch [23].

An important parameter of the OSSB modulation is the power of the RF component beat by the carrier and the first-order sideband, because the information is carried by the first-order sideband in the long-reach RoF system, and the response of the device under test (DUT) is also carried by the first-order sideband in the high-resolution optical vector network analysis. By beating the first-order sideband with the optical carrier, the information is transferred to the electrical domain, which can be detected or processed using the mature RF technologies.

For the OSSB modulation based on the 120° hybrid coupler, the optical fields of the carrier and the +1st-order sideband can be expressed as

$$\begin{cases} E_{0,120} = \sqrt{3} E_c J_0(\beta) \exp\left[i\left(\omega_c t + \frac{\pi}{6}\right)\right] \\ E_{+1,120} = \sqrt{3} E_c J_1(\beta) \exp\left[i(\omega_c t + \omega_e t + \pi)\right]. \end{cases} \tag{6}$$

The electric field of the RF signal beat by the carrier and the +1st-order sideband can be written as

$$\begin{aligned} E_{\mathrm{RF},120} &= \eta\left(E^*_{0,120} \cdot E_{+1,120} + E^*_{+1,120} \cdot E_{0,120}\right) \\ &= 6\eta E_c^2 J_0(\beta) J_1(\beta) \cos\left(\omega_e t + \frac{5\pi}{6}\right) \end{aligned} \tag{7}$$

where η is the responsivity of the PD.

Similarly, the optical fields of the carrier and the +1st-order sideband in the conventional OSSB modulation based on the 90° hybrid coupler can be expressed as

$$\begin{cases} E_0^{90} = \sqrt{2} E_c J_0(\beta) \exp\left[i\left(\omega_c t + \frac{\pi}{4}\right)\right] \\ E_{+1}^{90} = 2 E_c J_1(\beta) \exp\left[i(\omega_c t + \omega_e t)\right]. \end{cases} \tag{8}$$

The electric field of the corresponding RF signal beat by the carrier and the +1st-order sideband has the form of

$$\begin{aligned} E_{\mathrm{RF},90} &= \eta\left(E^*_{0,90} \cdot E_{+1,90} + E^*_{+1,90} \cdot E_{0,90}\right) \\ &= 4\sqrt{2}\eta E_c^2 J_0(\beta) J_1(\beta) \cos\left(\omega_e t - \frac{\pi}{4}\right). \end{aligned} \tag{9}$$

The power ratio of the two RF signals is

$$\frac{P_{\mathrm{RF},120}}{P_{\mathrm{RF},90}} = \frac{9}{8} \approx 0.512 \text{ dB}. \tag{10}$$

With the same modulation indices, the power of the RF signal beat by the carrier and the +1st-order sideband in the proposed OSSB modulation is 0.512-dB larger than that in the conventional OSSB modulation.

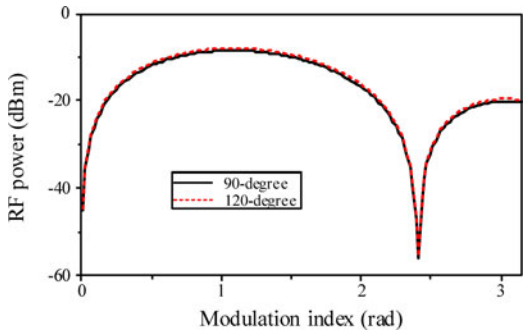

Fig. 3. The powers of the RF components beat by the optical carrier and the +1st-order sideband of the OSSB signals generated by the proposed and the conventional schemes as a function of the modulation index.

Fig. 3 shows the powers of the RF components beat by the optical carrier and the +1st-order sideband of the OSSB signals generated by the proposed and the conventional schemes as a function of the modulation index. In the calculation, the power of the input optical signal is 10 dBm and the responsivity of the PD is 0.8 A/W. As can be seen, the RF component beat by the carrier and the +1st-order sideband of the OSSB signal generated by the proposed scheme is generally 0.512-dB larger than that of the OSSB signal generated by the conventional scheme, which reaches its peak at a phase modulation index of 1.09.

In addition, the optical power of the OSSB signal is also important in the long-reach RoF system. For the OSSB signal generated by the proposed modulation scheme, the optical field can be written as

$$\begin{aligned} E_{120}(t) = {} & E_c \exp(i\omega_c t)\left\{\exp\left[i\beta\cos\left(\omega_e t + \frac{2\pi}{3}\right)\right]\right. \\ & \left. + \exp\left[i\beta\cos(\omega_e t) + i\frac{\pi}{3}\right]\right\} \end{aligned} \tag{11}$$

so the optical power is

$$P_{120} = E_{120}(t) \cdot E_{120}(t)^* = E_c^2\left[2 + J_0\left(\sqrt{3}\beta\right)\right]. \tag{12}$$

As a comparison, in the conventional OSSB modulation based on the 90° hybrid coupler, the optical power is given by

$$P_{90} = 2E_c^2. \tag{13}$$

Fig. 4 shows the optical powers of the OSSB signals as a function of the modulation index. The OSSB signals generated by the proposed and the conventional schemes have the same optical power when the modulation index is 1.39. Because the practical modulation index would be smaller than 1.39, the optical power of the OSSB signal generated by the proposed scheme is generally larger than that of the OSSB signal generated by the conventional scheme. At a phase modulation index of $\pi/3$, which is a practical value in a long-reach RoF system, the power of the OSSB signal generated by the proposed scheme is 0.84-dB larger than that of the OSSB signal generated by the conventional scheme.

In the proposed scheme, we have assumed that the RF powers to the two RF ports are identical and the phase difference

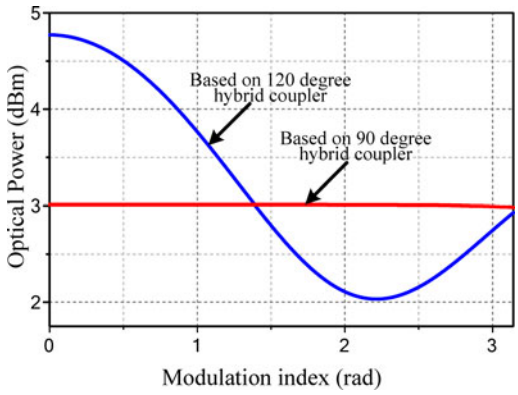

Fig. 4. The optical powers of the OSSB signals as a function of the modulation index.

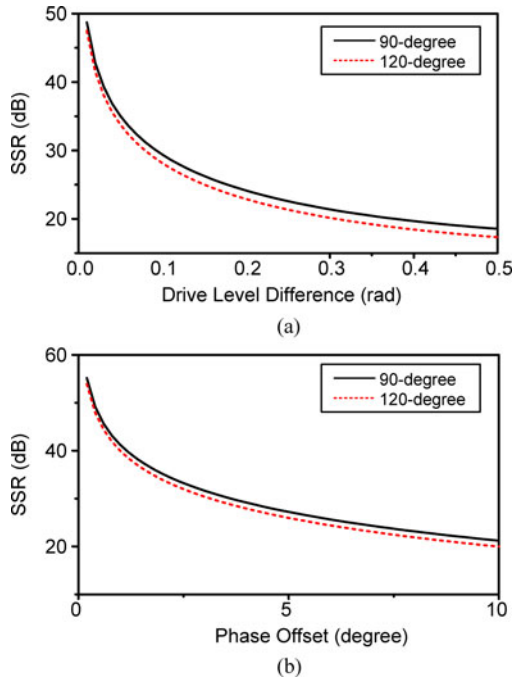

Fig. 5. The sensitivity of the proposed and conventional OSSB signals as a function of (a) the drive level difference and (b) the phase offset when the phase index is 1.

is exactly controlled, which is hard to achieve in practice. To evaluate the sensitivity of the proposed OSSB modulation on the drive level differences and phase offsets between the two drive signals, a simulation is performed. Fig. 5 shows the sideband suppression ratios (SSRs), i.e., the ratio of the desired first-order sideband to the undesired one, of the OSSB signals based on the 120° hybrid coupler and 90° hybrid coupler as a function of the drive level differences and phase offset. As can be seen, the SSR of the conventional OSSB modulation based on a 90° hybrid coupler is generally larger than that of the proposed OSSB modulation with the same phase offset, but the trends for both schemes are the same.

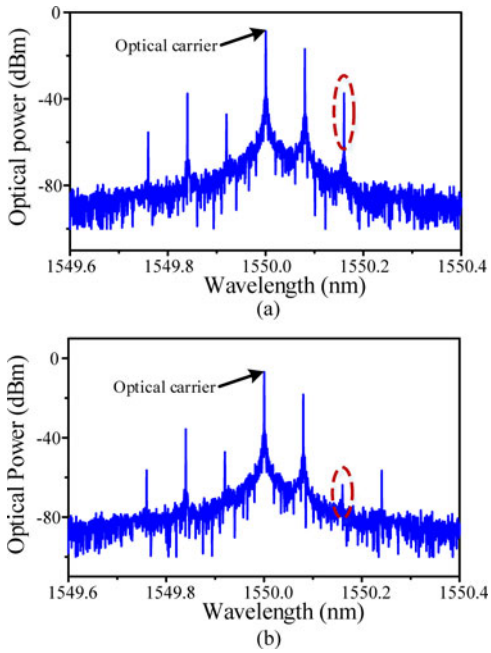

Fig. 6. The simulated optical spectrum of the OSSB modulated signals based on (a) the 90° hybrid coupler and (b) the 120° hybrid coupler when the modulation index is $\pi/3$.

III. Simulation and Experimental Results

In order to demonstrate the concept and to evaluate the performance of the proposed scheme, a comparative numerical simulation and experimental study between the conventional OSSB modulation and the proposed OSSB modulation is carried out.

In the simulation, the extinction ratio of the dual-drive MZM is 30 dB, the line-width of the LD is 1 MHz, and the frequency of the RF signal is 10 GHz. The 90° and 120° hybrid couplers are ideal, which can split a RF signal into two parts with equal powers and an exact phase difference of 90° or 120°.

In the experiment, a vector signal generator (Agilent E8267D) and a tunable laser source (Agilent N7714A) are used as the RF source and the optical source, respectively. The dual-drive MZM (Fujitsu FTM7921ER) has a 3-dB bandwidth of 10 GHz and a half-wave voltage of 2.6 V. The optical spectrum of the modulated signal is observed by an optical spectrum analyzer (Yokogawa AQ6370C) with a resolution of 0.02 nm, and the EVM is measured by an electrical signal analyzer (Agilent N9030A).

A. The Optical Spectrum

Fig. 6 shows the simulated optical spectrum of the OSSB signals based on the 90° hybrid coupler and the 120° hybrid coupler. Because of the limited extinction ratio of the modulator, the -1st-order sideband is not completely suppressed. For both of the two OSSB modulations, the suppression ratio of the -1st-order sideband is almost the same. But the $+2$nd-order sideband of the proposed OSSB modulation is 26.38-dB lower than that of the conventional OSSB modulation when the modulation index is $\pi/3$.

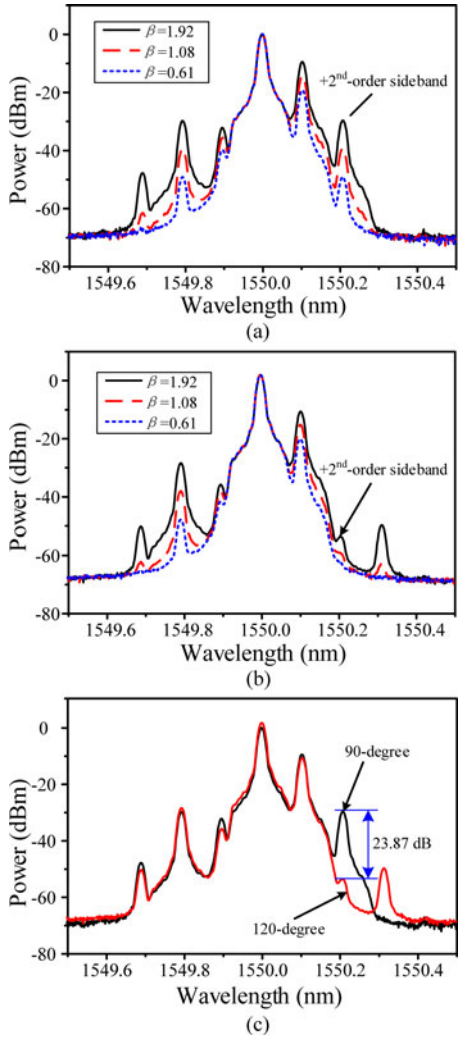

Fig. 7. The experimentally measured optical spectra of the OSSB-modulated signals based on (a) the 90° hybrid coupler and (b) the 120° hybrid coupler. (c) The optical spectra of the conventional and the proposed OSSB signals with a modulation index of 1.92.

The simulation result is validated by the experiment. Fig. 7 shows the experimentally measured optical spectra of the OSSB signals at different phase modulation indices. From Fig. 7(a) and (b), it is obvious that the −1st-order sidebands of the two OSSB modulations are greatly suppressed, while the powers of the +2nd-order sideband of the proposed OSSB signals are 23.87, 19.92, and 14.08-dB lower than those of the conventional ones when the phase modulation indices are 1.92, 1.08, and 0.61, respectively.

B. The Performance in OSSB-Based OVNA

When an OSSB signal propagates through a DUT, the DUT would change the phase and magnitude of each sideband in the OSSB signal. Converting the OSSB signal back to a RF signal, the change of the phase and magnitude can be accurately extracted by a RF phase-magnitude detector. By scanning the frequency of the RF signal, the phase and magnitude responses of the DUT can be obtained. Optical vector network analysis

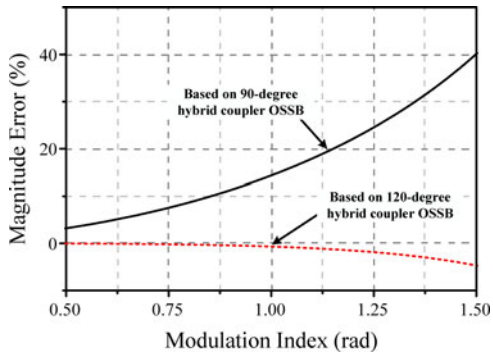

Fig. 8. The simulated measurement error of the magnitude response.

is thus realized [4]–[9]. Although the OSSB-based OVNA can have very high resolution in principle, the measurement accuracy is limited by the high-order sidebands of the OSSB signal. The +2nd-order sideband, which has the highest power among all the high-order sidebands, introduces the maximum measurement error [20], [21]. Since the proposed OSSB modulation scheme can effectively suppress the +2nd-order sideband, it should improve significantly the performance of the OSSB-based OVNA. By assuming the response of the DUT as $H(\omega) = 1$, the measurement error of the magnitude response as a function of the modulation index is calculated, with the results shown in Fig. 8. It can be seen that the measurement result using the conventional OSSB modulation is always bigger than the actual value. However, the error is close to zero if the proposed OSSB modulation is used. At a phase modulation index of $\pi/3$, the errors are 16.05% and –0.81% for the conventional and proposed OSSB modulation schemes, respectively.

Since the transfer function is assumed to be $H(\omega) = 1$, the phase of the components beat by the mth and $(m+1)$th-order sidebands are always equal. As a result, we cannot find the measurement errors in phase. To study the errors of the phase measurement, a complex $H(\omega)$ must be assumed. Fig. 9 shows the ideal responses of the PS-FBG and the calculated responses of the PS-FBG by the OVNA based on the conventional and proposed OSSB modulations. The notch depth of the actual PS-FBG is 27.85 dB and the phase shift is 180°. From Fig. 9, the magnitude and phase responses of the PS-FBG obtained by the OVNA based on the proposed OSSB modulation almost coincide with the ideal responses, while the responses achieved by the OVNA based on the conventional OSSB modulation is obviously deviated from the actual ones.

C. The Performance in Long-Distance RoF System

Due to the low insertion loss and wide bandwidth of the optical fiber, RoF system is an attractive approach for distributing high frequency wireless signals. However, the performance of the RoF system is restricted by the chromatic dispersion of the optical fiber, which would lead to serious frequency-dependent power fading if the optical microwave signal is a DSB signal. By applying the OSSB modulation, the RoF system can be free from the effect of the fiber dispersion. However, the

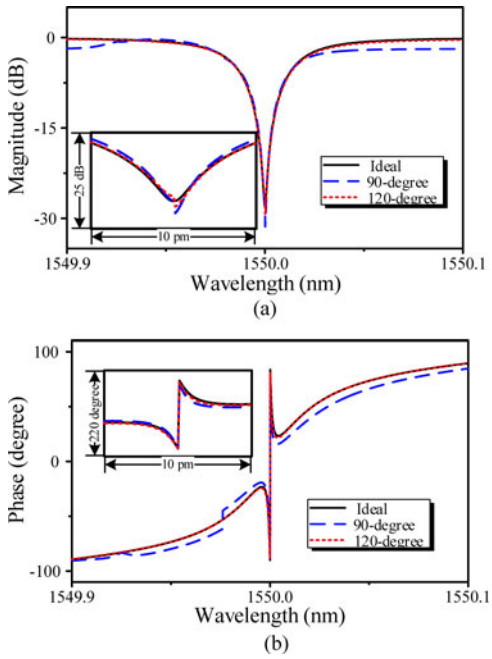

Fig. 9. The ideal response and the calculated responses of the PS-FBG when the phase modulation index is 1. (a) Magnitude response, (b) phase response. The insets: zoom-in view of the responses at the notch of the PS-FBG.

TABLE I
THE TRANSMISSION PERFORMANCE OF THE TWO OSSB SIGNALS

	Conventional OSSB Modulation	Proposed OSSB Modulation
Back-to-back EVM_{rms}/%	3.9318	3.7953
EVM_{rms} of the signal transmitted by 20-km single mode fiber/%	4.4790	4.1778

conventional OSSB signals always contain undesirable high-order sidebands. For instance, there are three consecutive spectral lines in Fig. 7(a), so the signal can also be seen as a DSB signal, which would be affected by the fiber dispersion as well. In the proposed OSSB modulation, the generated signal has only two consecutive spectral lines, which should have better transmission performance over long distance optical fiber.

In order to compare the transmission performance of the two OSSB signals, a RoF link with a 20-km SMF is constructed. The optical carrier from the laser source is fixed at 10 dBm, and the power and frequency of the drive microwave signal are 12 dBm and 10 GHz, respectively. The RF signal is modulated by a 50 Mbaud 16 QAM digital signal.

Table I illustrates the rms value of the EVM before and after the 20-km SMF transmission. As can be seen, the EVM difference is 0.1365% for the back-to-back case. After the 20-km SMF transmission, the EVM of the OSSB signal generated by the proposed and conventional scheme are degraded by 0.3825% and 0.5472%, respectively, showing that the proposed OSSB modulation scheme has a better transmission performance in the long-reach RoF system.

IV. CONCLUSION

A novel OSSB modulation scheme based on a 120° hybrid coupler and a dual-drive MZM was proposed and demonstrated. According to the analytical analysis, simulation results, and experiment measurement, the −1st and +2nd-order sidebands (or the +1st and −2nd-order sidebands) in the generated OSSB signal were effectively suppressed. Because the +2nd-order sideband was greatly suppressed in the proposed OSSB modulation, the measurement accuracy of the OSSB-based OVNA was greatly improved. The proposed OSSB modulation also had better transmission performance than the conventional scheme using 90° hybrid coupler. In addition, the power of the RF component beat by the carrier and the +1st-order sideband of the proposed OSSB modulation is 0.512-dB larger than that of the conventional one.

REFERENCES

[1] Z. Z. Cao, J. J. Yu, L. Chen, and Q. L. Shu, "Reversely modulated optical single sideband scheme and its application in a 60-GHz full duplex ROF system," *IEEE Photon. Technol. Lett.*, vol. 24, no. 10, pp. 827–829, May 2012.

[2] T. G. Ning, J. Li, L. Pei, F. Zhang, Q. A. Zhou, X. D. Wen, C. H. Qi, and J. J. Zheng, "Overwritten fiber Bragg grating and its application in an optical single sideband with carrier modulation radio over a fiber system," *Opt. Eng.*, vol. 50, pp. 035001-1–035001-5, Mar. 2011.

[3] H. J. Zhou, W. Chen, and Z. Meng, "Optical single sideband-frequency generation with carrier totally suppressed for Brillouin distributed fiber sensing," *Opt. Commun.*, vol. 285, pp. 4391–4394, 2012.

[4] J. E. Román, M. Y. Frankel, and R. D. Esman, "Spectral characterization of fiber gratings with high resolution," *Opt. Lett.*, vol. 23, pp. 939–941, 1998.

[5] D. J. Krause, J. C. Cartledge, L. Jakober, and K. Roberts, "Measurement of passive optical components using a carrier and single sideband," in *Proc. Opt. Fiber Commun./Nat. Fiber Opt. Eng. Conf.*, 2006, pp. 2612–2614.

[6] Z. Z. Tang, S. L. Pan, and J. P. Yao, "A high resolution optical vector network analyzer based on a wideband and wavelength-tunable optical single-sideband modulator," *Opt. Exp.*, vol. 20, pp. 6555–6560, 2012.

[7] S. L. Pan and M. Xue, "Optical vector network analyzer based on optical single-sideband modulation," presented at the 12th Int. Conf. Optical Communications and Networks, Chengdu, China, 2013, paper SC3In7.

[8] M. Sagues, M. Pérez, and A. Loayssa, "Measurement of polarization dependent loss, polarization mode dispersion and group delay of optical components using swept optical single sideband modulated signals," *Opt. Exp.*, vol. 16, no. 20, pp. 16181–16188, 2008.

[9] W. Li, W. H. Sun, W. T. Wang, L. X. Wang, J. G. Liu, and N. H. Zhu, "Reduction of measurement error of optical vector network analyzer based on DPMZM," *IEEE Photon. Technol. Lett.*, vol. 26, no. 9, pp. 866–869, May 2014.

[10] H. Mima and K. Iwashita, "A novel wavelength converter based on optical single-sideband modulator and arrayed waveguide grating," in *Proc. Opto-Electron. Commun. Conf.*, 2012, pp. 327–328.

[11] T.Yamamoto, R. Kohno, A. Chiba, T. Sakamoto, and T. Kawanishi, "Agile wideband light source for optical coherence tomography using optical SSB frequency sweep technique," in *Proc. Dig. IEEE/LEOS Summer Top. Meet.*, 2007, pp. 137–138.

[12] Z. Li, H. Chi, X. M. Zhang, and J. P. Yao, "Optical single-sideband modulation using a fiber-Bragg-grating-based optical Hilbert transformer," *IEEE Photon. Technol. Lett.*, vol. 23, no. 9, pp. 558–560, May 2011.

[13] S. R. Blais and J. P. Yao, "Optical single sideband modulation using an ultranarrow dual-transmission-band fiber Bragg grating," *IEEE Photon. Technol. Lett.*, vol. 18, no. 21, pp. 2230–2232, Nov. 2006.

[14] A. A. Savchenkov, W. Liang, A. B. Matsko, V. S. Ilchenko, D. Seidel, and L. Maleki, "Tunable optical single-sideband modulator with complete sideband suppression," *Opt. Lett.*, vol. 34, pp. 1300–1302, 2009.

[15] M. Sagues and A. Loayssa, "Swept optical single sideband modulation for spectral measurement applications using stimulated Brillouin scattering," *Opt. Exp.*, vol. 18, pp. 17555–17568, 2010.

[16] Y. Ogiso, Y. Tsuchiya, S. Shinada, S. Nakajima, T. Kawanishi, and H. Nakajima, "High extinction-ratio integrated Mach-Zehnder modulator

with active Y-branch for optical SSB signal generation," *IEEE Photon. Technol. Lett.*, vol. 22, no. 12, pp. 941–943, Jun. 15, 2010.
[17] B. Hraimel, X. P. Zhang, Y. Q. Pei, K. Wu, T. L. Liu, T. F. Xu, and Q. H. Nie, "Optical single-sideband modulation with tunable optical carrier to sideband ratio in radio over fiber systems," *J. Lightw. Technol.*, vol. 29, no. 5, pp. 775–781, Mar. 2011.
[18] J. Cviklinski, J. Ortalo, J. Laurat, A. Bramati, M. Pinard, and E. Giacobino, "Reversible quantum interface for tunable single-sideband modulation," *Phys. Rev. Lett.*, vol. 101, p. 133601, 2008.
[19] A. A. Savchenkov, A. B. Matsko, W. Liang, V. S. Ilchenko, D. J. Seidel, and L. Maleki, "Single-sideband electro-optical modulator and tunable microwave photonic receiver," *IEEE Trans. Microw. Theory Tech.*, vol. 58, no. 11, pp. 3167–3174, Nov. 2010.
[20] M. Xue, Y. J. Zhao, X. W. Gu, and S. L. Pan, "Performance analysis of optical vector analyzer based on optical single-sideband modulation," *J. Opt. Soc. Amer. B*, vol. 30, pp. 928–933, 2013.
[21] R. Hernandez, A. Loayssa, and D. Benito, "Optical vector network analysis based on single-sideband modulation," *Opt. Eng.*, vol. 43, pp. 2418–2421, 2004.
[22] A. M. Abbosh, "Ultra-wideband phase shifters," *IEEE Trans. Microw. Theory Tech.*, vol. 55, no. 9, pp. 1935–1941, Sep. 2007.
[23] M. Naser-Moghadasi, G. R. Dadashzadeh, A. M. Dadgarpour, F. Jolani, and B. S. Virdee, "Compact ultra-wideband phase shifter," *Prog. Electromagn. Res. Lett.*, vol. 15, pp. 89–98, 2010.

Min Xue was born in Changzhou, China, in September 1988. He received the B. S. degree from the College of Electronic and Information Engineering, Nanjing University of Aeronautics and Astronautics, Nanjing, China, in 2011, and is currently working toward the Ph.D. degree in the same college. His research interests include photonic microwave measurement and metrology, optical fiber sensor, and integrated microwave photonic devices.

Shilong Pan (S'06–M'08–SM'13) received the B.S. and Ph.D. degrees in electronics engineering from Tsinghua University, Beijing, China, in 2004 and 2008, respectively.

He joined the College of Electronic and Information Engineering, Nanjing University of Aeronautics and Astronautics, Nanjing, China, in 2010, where he is currently a Professor and Executive Director of the Key Laboratory of Radar Imaging and Microwave Photonics, Ministry of Education. From 2008 to 2010, he was a "Vision 2010" Postdoctoral Research Fellow in the Microwave Photonics Research Laboratory, University of Ottawa, Ottawa, ON, Canada. He has authored or coauthored more than 160 papers, including more than 90 papers in peer-reviewed journals and more than 60 papers in conference proceedings. His research interests include microwave photonics, which includes UWB over fiber, radio over fiber, photonic generation of microwave, Millimeter wave, and terahertz, photonic processing of microwave signals, photonic microwave measurement, and integrated microwave photonic devices.

Dr. Pan is a member of the Optical Society of America.

Yongjiu Zhao's biography not available at the time of publication.